Electronic Materials Letters (2023) 19:543–553
https://doi.org/10.1007/s13391-023-00430-7

ORIGINAL ARTICLE - NANOMATERIALS

Compressive Sinter Bonding in Air Between Cu Finishes Using Paste Containing Composite Ag_2O-Cu Filler

Byeong Jo Han[1] · **Jong-Hyun Lee**[1]

Received: 20 January 2023 / Accepted: 27 March 2023 / Published online: 6 April 2023

Abstract

A Ag_2O-Cu composite filler was adopted as a sintering material between Cu finishes under compression to achieve the high-speed bonding of dies in an air atmosphere via a cost-effective paste and finish process. The commercial Cu particles had an average size of 2 μm, and the synthesized Ag_2O particles were in the submicrometer range with an average size of 210 nm. The Ag_2O particles in the paste started decomposing at ~150 °C, and the liquid-type reductant in the paste effectively reduced the oxide layers on the Cu particles as well as the upper and lower Cu finishes during bonding. Therefore, the in situ-generated active Ag and fresh Cu surfaces enabled significantly rapid sinter bonding under 5 MPa compression. Only 30 s of bonding at 300 °C was required to achieve an excellent shear strength of 27.8 MPa in the created bond-line, while 90 s of bonding produced a near-full-density structure with a strength of 41.9 MPa despite solid-state sintering when the 3:7 (Cu particles:Ag_2O particles) mixing ratio was used. Well-dispersed Ag_2O particles did not create a non-sintered interface or form large voids upon outgassing during decomposition. The out-diffused Cu was reoxidized after sintering with Ag, forming irregularly dispersed Cu_2O shells that remained in the microstructure of the full-density bond-line.

Graphical Abstract

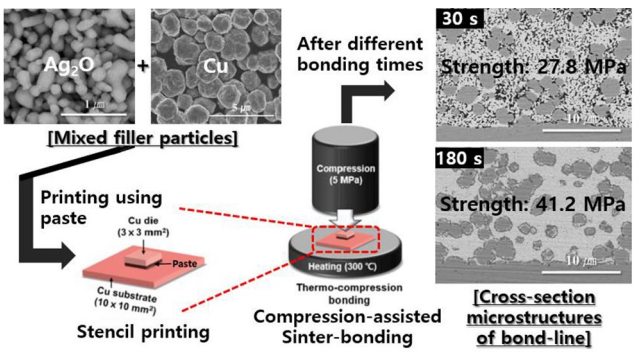

Keywords Die-attach · Silver oxide-copper composite paste · High-speed sinter bonding · Silver oxide decomposition · Copper oxide reduction

✉ Jong-Hyun Lee
pljh@snut.ac.kr

[1] Department of Materials Science and Engineering, Seoul National University of Science and Technology, 232 Gongneung-ro, Nowon-gu, Seoul 139-743, Republic of Korea

1 Introduction

The wide-scale applications of wide-bandgap semiconductors (e.g., SiC), including in heat-generating devices and high-power light emitting diodes (LEDs), have led to the advent of sinter bonding in die-attach technology, replacing soldering [1–6]. In these applications, the temperature is significantly elevated in the formed bond-line during operation, with a possibility of inducing serious reliability issues for the bond-line that comprises a low-melting-point metal, such as solder [7–9].

Ag is an ideal bond-line metal owing to its high melting point (961 °C) and excellent thermal conductivity (406 W/m•K) [10]. Additionally, owing to its excellent sintering capabilities and oxidation resistance in air, Ag is highly preferred as a filler metal in pastes [11, 12]. Moreover, the sinterability between Ag particles has been improved by adopting nano-sized particles [5, 13–15]. Two research directions have been proposed to enhance the effectiveness of sinter bonding: compressionless sintering for multiple die-attach adhesives in a chamber [1–3, 5] and compression-assisted increase in the bonding speed for individual die-attach adhesives [1, 4–6, 13–16]. The main scope of this study falls under the latter direction.

Compression-assisted solid-state sintering using Ag nanoparticles generally requires long bonding times. Ide et al. reported a high-speed bonding approach, realized via 5 MPa-compression sinter bonding for 5 min at 300 °C using Ag nanoparticles (average size: 11 nm), achieving a high shear strength of ~40 MPa [13]; however, shortening the bonding period remains imperative. In this regard, Lee et al. recently suggested the usage of submicron Ag_2O particle fillers instead of pure Ag, which drastically reduces the bonding time [17]. Atom-scale active Ag, that was in situ generated through bonding via Ag_2O decomposition during heating [17–23], presented much better sinterability than pure Ag nanoparticles. As a result, a moderate shear strength of 21.4 MPa was obtained after a significantly short bonding time of 30 s at 200 °C [17]. However, there are still issues to be resolved, including the high cost of the 100% Ag_2O particle filler, the requirement for the fabrication of upper and lower Ag finishes by additional electroplating, and the development of non-sintered interfaces (e.g., long cracks) caused by decomposition-derived outgassing [17].

Here, high-speed die attachment was achieved via sinter bonding by using a composite-particle paste containing low-coat microscale Cu particles and Ag_2O particles between the Cu finishes. Two effective solvent-type reductants were used to enable paste mixing because the surfaces of the added Cu particles and Cu finishes were covered with oxide layers. The die-attach temperature was adjusted to 300 °C, where according to previous reports [24, 25], the bonding between the Cu particles and Cu finish becomes the strongest.

2 Materials and methods

The Ag_2O filler particles for the sinter-bonding paste were synthesized by exchanging a polyethylene glycol vehicle in a reported method [26] with deionized (DI) water [17]; the Cu particles (CUSP20, JoinM) were purchased. The two types of particles were mixed at a weight ratio of 4:6 or 3:7 (Cu:Ag_2O) for 3 min in ethanol (95%, Korea Alcohol Industrial Co.) via ultrasonication after stirring at 200 rpm. Subsequently, the suspension was dried for 12 h at 25 °C in a low-vacuum chamber after decanting.

Using a spatula, approximately 30 wt% of the mixed particles was combined with the mixed reductants to create the paste. The mixed reductants were prepared at a weight ratio of 6:4 with glycerol ($C_3H_8O_3$, 99%, Daejung Chemical & Metals Co.) and a polyol-based solvent (EW-10, Epsilon Epowder). The thermal behavior of the paste was examined via thermogravimetric and differential thermal analysis (TG-DTA, DTG-60, Shimadzu) at a heating rate of 20 °C•min^{-1}.

Die bonding was performed using a dummy Cu die and substrate; the dimensions of the die and substrate were 3 × 3 and 10 × 10 mm, respectively. The paste was stencil-printed onto the substrate by squeezing through a stencil mask with a 3 × 3 × 0.1 mm slit. Subsequently, the die was aligned on the printed pattern. The sandwich-structured sample was placed on a self-produced heating chuck and rapidly heated in air to 300 °C at 30 °C•s^{-1}. The sample was compressed at 5 MPa immediately after the start of heating for die bonding. The bonding time was measured promptly after the compression on the upper-side center of the die using a 14-mm diameter collet. The mechanical strength of the formed bond-line was measured as shearing strength by using a Dage-4000 bond tester system (Nordson DAGE). The strength was defined as the maximum stress value measured during shearing at 200 μm•s^{-1}. The initial position of the shearing tip was at a height of 200 μm from the substrate surface.

The morphologies of the used particles, cross-section microstructures of the bond-lines, and fracture surfaces after shearing were analyzed through high-resolution scanning electron microscopy (HR-SEM, SU8010, Hitachi). The cross-section microstructures and fracture surfaces were observed via back-scattered electron (BSE) imaging to clearly distinguish the Ag and Cu phases. The fine microstructures of both the added Cu particles and neighboring bond-lines were examined through transmission electron microscopy (TEM, JEM-ARM200F) conducted using a cold field-emission electron gun (JEOL Ltd.) operated at an acceleration voltage of 200 kV.

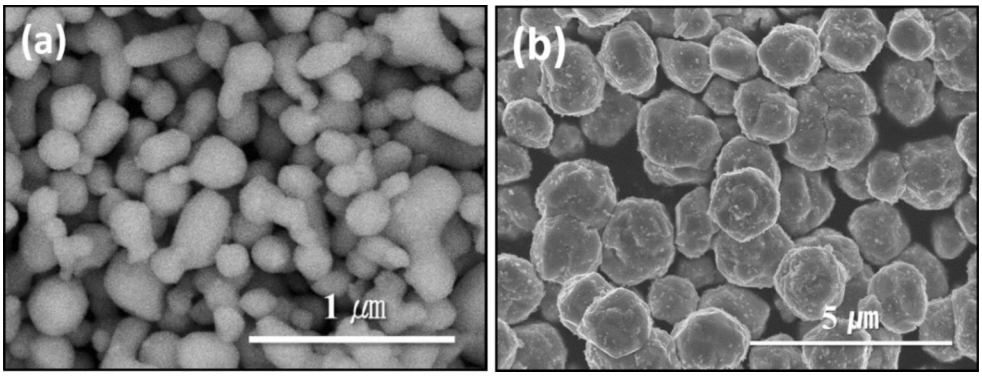

Fig. 1 **(a)** Ag_2O and **(b)** Cu particles used in this study

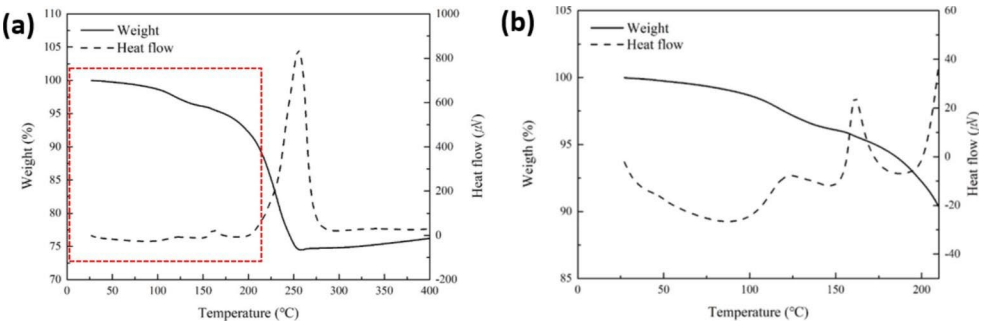

Fig. 2 **(a)** TG-DTA results of the prepared Cu-Ag_2O 3:7 paste and **(b)** enlarged curves of the dotted region in **(a)**

3 Results and Discussion

Figure 1(a) shows the morphologies of the synthesized Ag_2O particles. Despite their submicrometer size, irregular necked shapes were formed and local agglomeration was observed; moreover, the particle surfaces were considerably smooth. Figure 1(b) shows the commercial Cu particles with a ~ 2 μm average size. Despite having slightly irregular morphologies, their shapes were pseudo-spherical and their surfaces were rough.

Figure 2 shows the TG-DTA results for the fabricated 3:7 paste. Until 257 °C, accelerated weight loss occurred because of the vaporization of the reductant in the paste. The main exothermic peak was also observed at 255 °C owing to sintering between the particles. Additionally, weak endothermic peaks and an exothermic peak were observed at 146, 187, and 160 °C, respectively. Considering that the temperatures were within the weight loss range till up to 257 °C, the endothermic peaks were attributed to the vaporization of the reductant, while the exothermic peak was assigned to the redox reactions occurring in the paste, including the decomposition of Ag_2O [17]. The pure Ag_2O particles underwent weight loss by decomposing from temperatures exceeding 400 °C [18, 27, 28], while the solvent-containing paste underwent thermodynamic decomposition at much lower temperatures (with the formation of an endothermic peak) owing to the presence of carbons and hydrogens in the solvent [20, 29]. In a previous study [17], the paste containing Ag_2O particles and ethylene glycol exhibited an endothermic peak at 164 °C. Therefore, the different temperatures observed in the TGA results can be attributed to the changed paste formulation.

The shear strength as a function of the mixing ratio and bonding time, corresponding to sinter bonding at 300 °C at a compressive pressure of 5 MPa, is illustrated in Fig. 3. For a 4:6 mixing ratio, an extremely short bonding time of 30 s led to an insufficient shear strength of 10.6 MPa. The strength gradually increased as the bonding time increased to 180 s, where it reached its maximum value and remained there until 300 s. Meanwhile, the 3:7 paste bonded for 30 s reached a high strength of 27.8 MPa, which surpassed that of the joint soldered using a high-melting-point alloy (Pb-5Sn) [30] and that requiring attachment of power device chips [31]. The shear strength value further increased to 45.5 MPa as the bonding time increased to 150 s, and eventually saturated. The majority of the reported maximum strengths upon sinter bonding using Cu particles were < 40 MPa [5]. In view of this, the 3:7 paste demonstrated outstandingly fast sinter-bondability between low-cost Cu finishes.

Figure 4 displays the cross-sectional bond-line microstructures (including that of the Cu finish interface) obtained via the BSE mode, following compression-assisted sinter bonding at 300 °C, 5 MPa, and different bonding times (entire bond-lines are also presented as insets). Figure 4(a) displays the bond-line formed in the 4:6 paste after 30 s of bonding, in which the in situ-generated Ag upon Ag_2O decomposition, Ag nanoparticles formed upon Ag atom agglomeration, and sintered Ag nanoparticles can be collectively observed. The Ag atoms generated in situ during

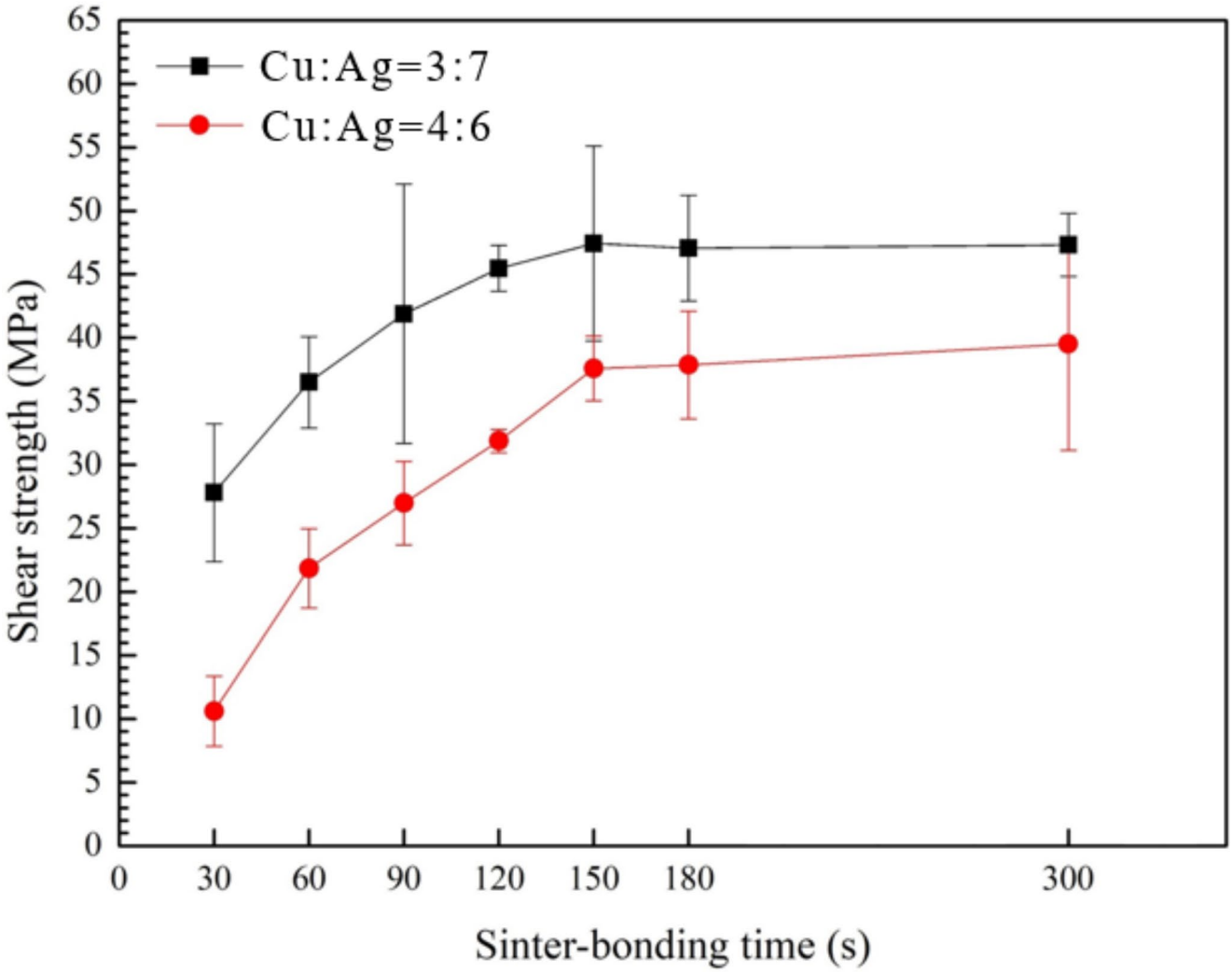

Fig. 3 Shear strength measured under different particle mixing ratios and bonding times during sinter bonding at 300 °C in air under 5 MPa compression

heating rapidly transformed to Ag nanoparticles, between which sintering occurred under compression. Some Ag nanoparticles were sintered with the upper and lower Cu finishes, where the surface oxide layers were removed by the mixed reductant [24, 25], which enabled the measurement of the shear strength. However, a porous structure with numerous voids was formed, because of outgassing and insufficient sintering. The Ag_2O particles surrounded by carbon and hydrogen atoms in the reductants were reduced according to Eq. (1) [20, 29]. Therefore, the formed CO_2 and H_2O escaped from the bond-line, preventing the sintering between Ag particles. Nevertheless, the outgassing did not result in the formation of significant voids in the bond-line, because the amount of gas per volume was reduced when Cu particles were added as opposed to when Ag_2O particles alone were used in the paste [17].

$$5Ag_2O+C_2H_4(OH)_2 \rightarrow 10Ag + 2CO_2+3H_2O \quad (1)$$

The bond-lines sinter-bonded for 60 and 90 s presented a porous structure with enhanced density and an improved sintering degree, even at the upper and lower interfaces. In contrast, an increase in the bonding time to 180 s under continuous compression induced significant microstructural changes in the density of the bond-line, including the interface regions. These microstructural characteristics reasonably explain the attained shear strength peak value. An increase in the bonding time to 300 s did not induce a noticeable microstructural change, which corresponded well with the saturation behavior of the shear strength. Therefore, it was inferred that with the increasing bonding time, the microstructural density of the bond-line formed at 300 °C and at 5 MPa rapidly increased until reaching full density, at which the shear strength was also maximized.

Figure 4(b) shows the magnified BSE bond-line images (including the Cu finish interface) with respect to the bonding time when the 3:7 paste was used. Although a porous

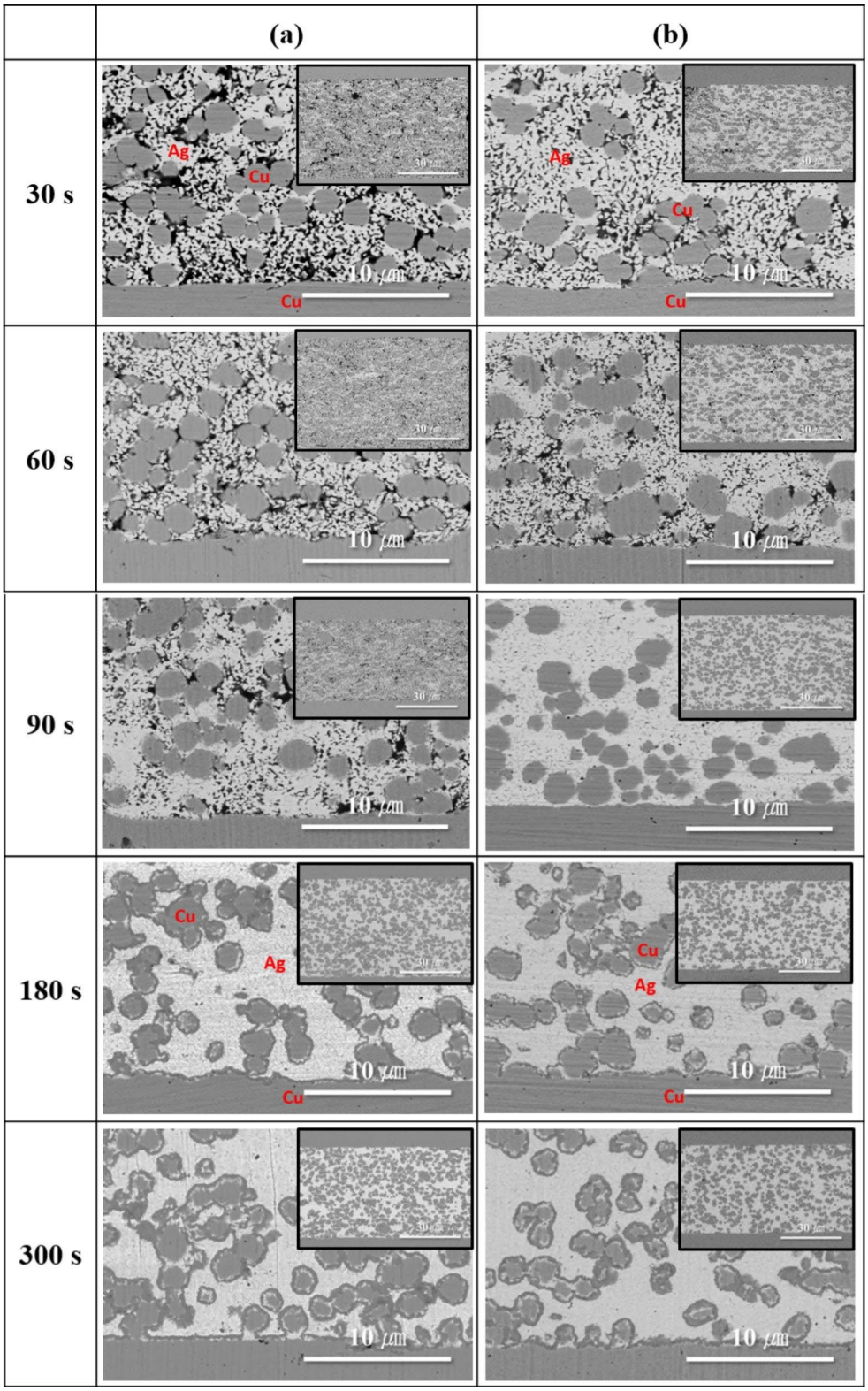

Fig. 4 Cross-section BSE images of the bond-lines with different bonding times under sinter-bonding at 300 °C and 5 MPa compression in air using **(a)** 4:6 and **(b)** 3:7 pastes

structure was observed over a short bonding time of 30 s, the microstructural density and sintering degree in the regions near the interface surpassed those of the 60 s-sintered bond-line in Fig. 4(a). This stemmed from the enhanced sintering between the Ag particles, which led to a higher measured shear strength value. Consequently, the enhancement in the microstructure can effectively explain the higher strength. Bonding for 60 s using the 3:7 paste further increased the

bond-line density. Accordingly, the 90 s-sintered bond-line approached a full-density state, while the 180 s-sintered bond-line exhibited a definite full-density state. Compared with the 180 s-sintered bond-line of the 4:6 paste in Fig. 5(a), the number of tiny voids between Ag grains in the 4:6 paste in Fig. 5(b) decreased, while the average Ag grain size was large, implying a more intense sintering state. These differences in the similar full-density state of the pastes contributed to the enhanced shear strength. Meanwhile, a 300 s-sintered bond-line resulted in a similar microstructure with full density, explaining the stagnation behavior of the shear strength. These results indicated that the high Ag_2O content of the 3:7 paste effectively elevated the densification speed of a bond-line structure.

To quantitatively confirm the densification degree in the bond-line of the 3:7 paste, the porosity of the bond-lines was measured relative to bonding time (Fig. 6). The pores in a cross-section image at ×1500 magnification were indexed using a self-production image analysis software (insets in Fig. 6), and the porosity was quantitatively calculated. According to the results, although the porosity of the 30 s-sintered bond-line was 4.52%, that of its 60 s-sintered equivalent decreased to 3.58%. The porosity eventually decreased to the near-full density state of only 0.09% after 90 s of sintering. For reference, the achieved porosity during compressive sinter bonding using Cu particles has been reported to vary in the range of several % to 10% [5].

Interestingly, the periphery of Cu particles in the full-density structures exhibited distinctive leopard-like spots, as shown in Fig. 7(a). Hence, energy dispersive spectrometry (EDS) elemental mapping images of the spots were obtained and analyzed through TEM. The brightest grey regions coincided with only the Ag detection map, implying the presence of pure Ag phases. Meanwhile, the darkest grey shell corresponded to the Cu and O detection maps, while only Cu was detected in the blotchy core region. Therefore, the darkest grey shell was determined as a copper oxide phase, and the core region was confirmed as the polycrystalline Cu phase. The quantitative EDS measurement results in the P1 and P2 regions (summarized in Fig. 7(b)) further verified that the darkest grey shell was a copper oxide phase. The atomic ratios of copper and oxygen atoms indicated that the oxide phase was Cu_2O. Furthermore, fast Fourier transform (FFT) analysis in the local region of the shell interior proved again that the shell comprised a polycrystalline Cu_2O phase (Fig. 8). Thus, the Cu_2O shell was inferred to have been formed by the oxidation of Cu, which was out-diffused across the in situ-produced sintered Ag particles on the reduced Cu surface under compression at 300 °C [32]. Additionally, because of the out-diffusion of Cu, microscopic holes were observed near the unevenly thick sintered Ag layer in the leopard-spot-based TEM image [32]. Tiny voids were also observed at the Cu_2O shell/outer Ag interface, stemming from the imperfect solid-state sintering; however, these voids had zero impact on the shear strength, as they were much smaller than the interparticle void formed during solid-state sintering [4, 6, 13].

The optical and SEM images of the die fracture surface, caused by the shear tests, are displayed as a function of the particle mixing ratio and bonding time in Fig. 9. All fracture modes in the 6:4 paste were determined as mixed mode (▲ mark). Although the highest fracture degree occurred within the bond-line, partial fracturing was observed at the upper Cu finish/bond-line interface (Fig. 9(a)). The BSE images of the fracture surface at the bond-line region near the interface are summarized in Fig. 9(b). Considering that Ag is the main phase governing the sinter-bonding properties, we specifically observed the cover area of the remaining Ag in the BSE image. The cover area of the bright grey Ag phase showed an upward trend with the increasing bonding time. Particularly, the 180 s-sintered sample with the full-density bond-line exhibited partially elongated fracture surfaces, as well as an abruptly increased cover area.

The 60 s-sintered sample with the 3:7 paste also showed mixed-mode fracturing (Fig. 9(c)). In contrast, the 180–300 s-sintered samples exhibited a cohesive fracturing mode (● mark), indicating that fracturing occurred entirely within the bond-line. Furthermore, these samples showed a more uniformly distributed elongated Ag fracture surface, whereas local fracturing was observed on the 60 s-sintered sample (Fig. 9(d)). Also, the observed fracture

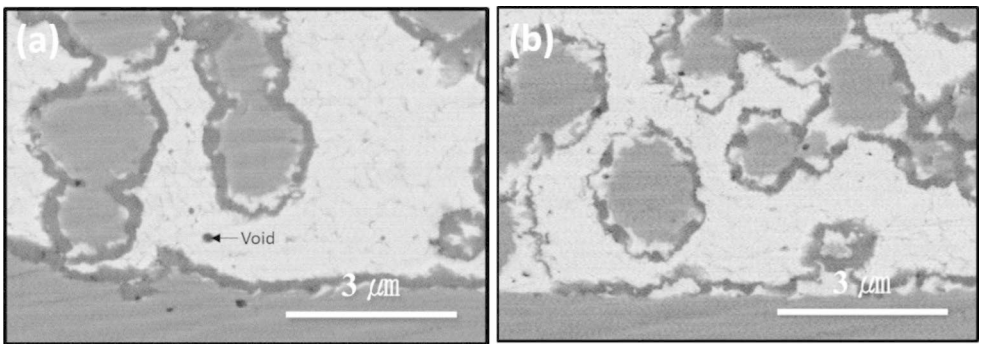

Fig. 5 Enlarged cross-section BSE images of the bond-lines sintered for 180 s under 5 MPa compression at 300 °C in air using **(a)** 4:6 and **(b)** 3:7 pastes

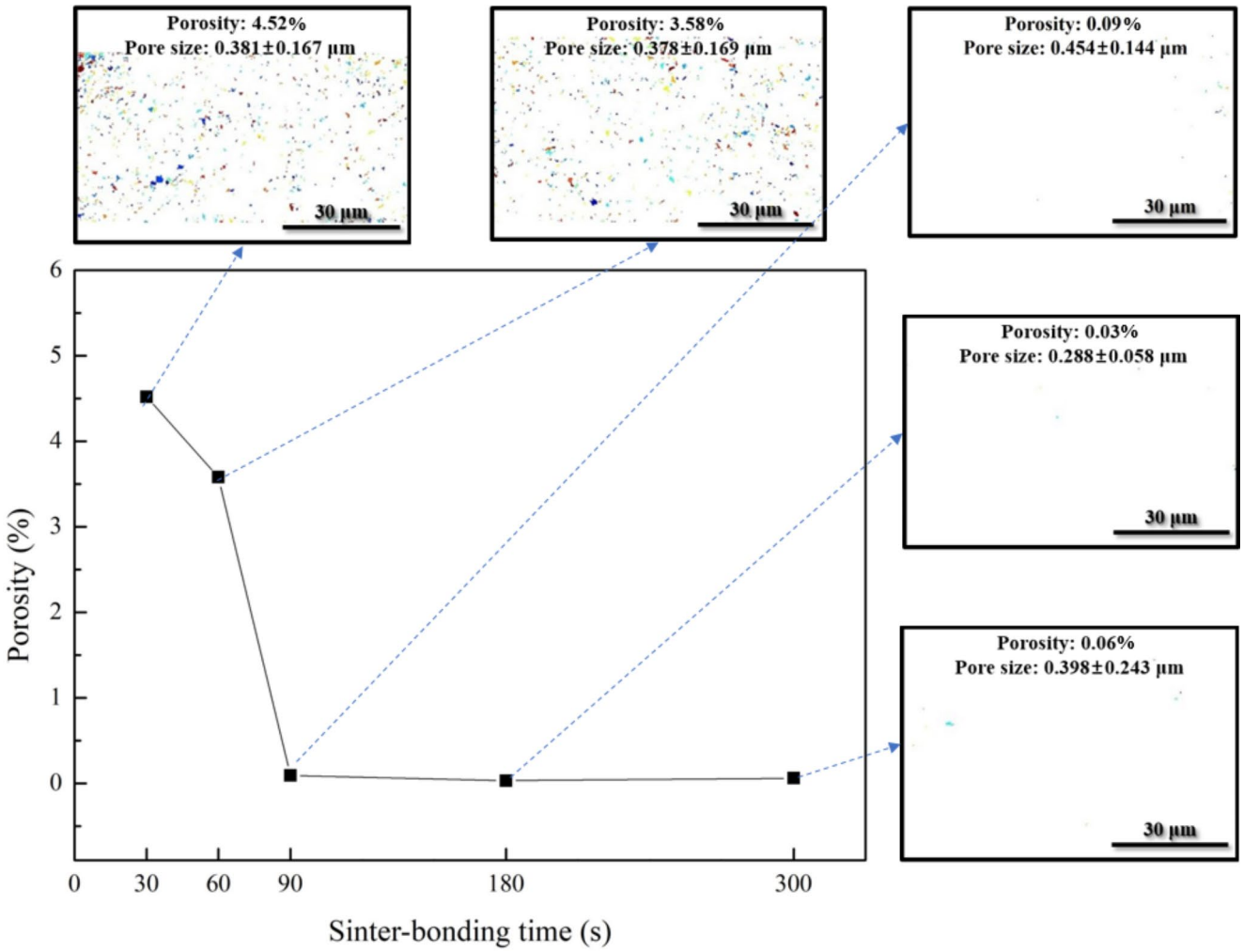

Fig. 6 Porosities measured in the bond-lines with different bonding times when the sinter-bonding was performed under 5 MPa compression at 300 °C in air using the 3:7 paste

characteristics corresponded well with the shear strength values, with respect to the paste type and bonding time.

4 Conclusions

Rapidly formed bond-lines for mass-produced die attachment was achieved by employing a composite paste containing Ag_2O and Cu particles, along with low-cost Cu paste and upper/lower Cu finishes, and sinter bonding at 300 °C under 5 MPa compression in air. The 210 nm Ag_2O particles in the paste started to decompose at ~150 °C, generating in situ active Ag nanoparticles for subsequent sintering. Furthermore, the paste contained mixed reductants that effectively eliminated the oxide surfaces on both the Cu particles and Cu finishes during bonding. The 3:7 paste (Cu:Ag_2O) samples sintered for 30 and 90 s both presented bond-line microstructures with typical porosity and near-full density, and achieved a shear strength of 27.8 and 41.9 MPa, respectively. Further, the outgassing of the Ag_2O particles in the paste during decomposition eliminated complications such as a non-sintered interface or the formation of long cracks and large voids. After sintering with Ag, the Cu particle surfaces were out-diffused and reoxidized, finally resulting in the irregular distribution of Cu_2O shells with core Cu phases in the full-density bond-line. The formed Ag-Cu composite bond-line exhibited both excellent thermal conductance and mechanical durability even at high temperatures (300 °C).

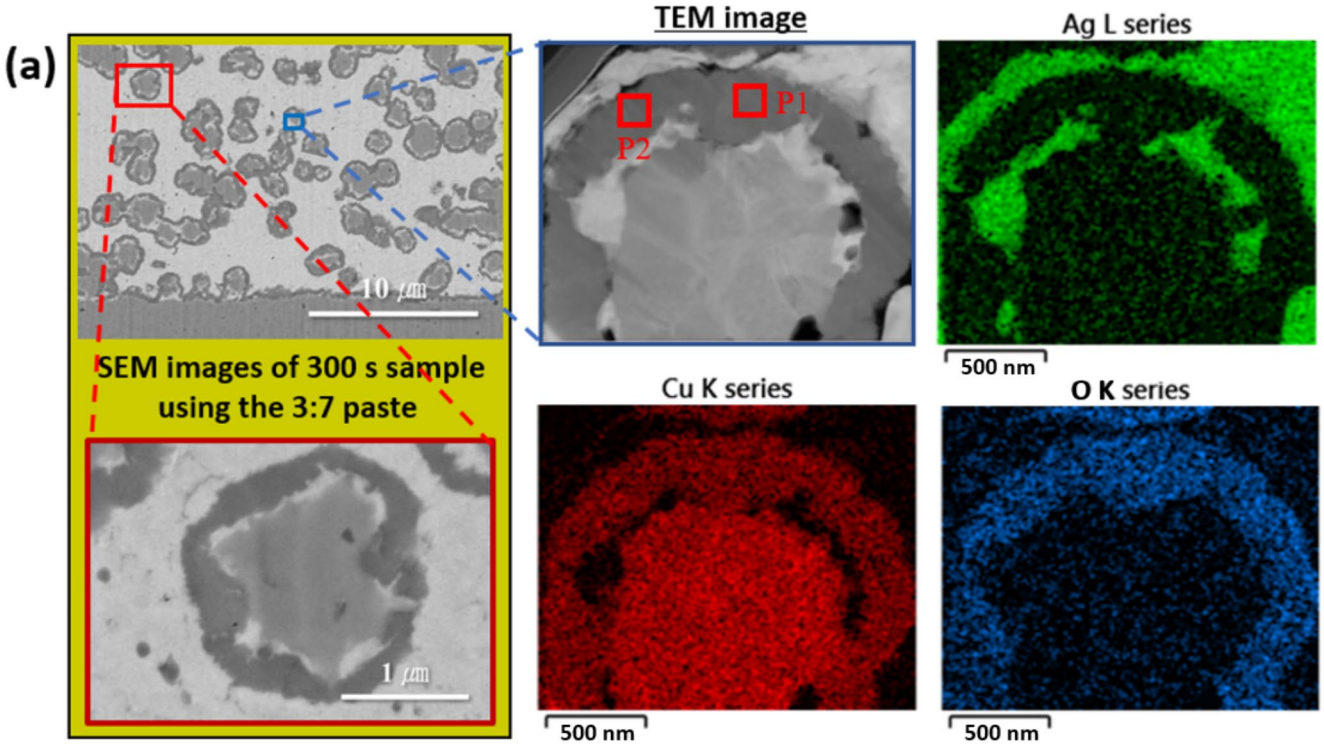

(b)

		Ag	Cu	O
At%	P1	0.32	65.96	33.72
	P2	2.72	64.51	32.77

→ Cu_2O

Fig. 7 **(a)** High-magnification cross-section BSE images of the bond-line and EDS elemental mapping images from the TEM work, and **(b)** EDS measurement results at P1 and P2 regions in **(a)**

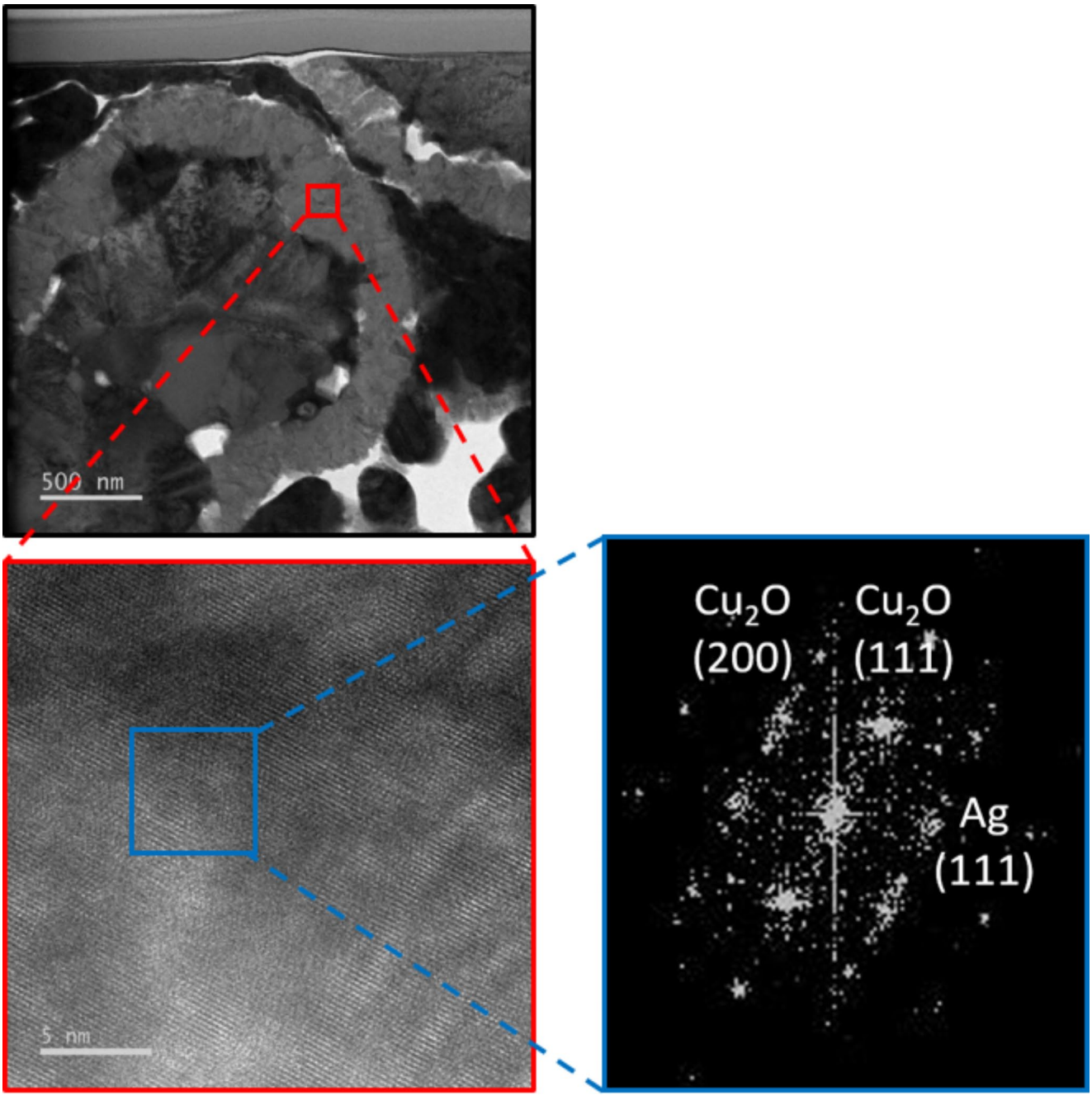

Fig. 8 Low- and high-magnification TEM image and FFT result in the O detection region of Fig. 7

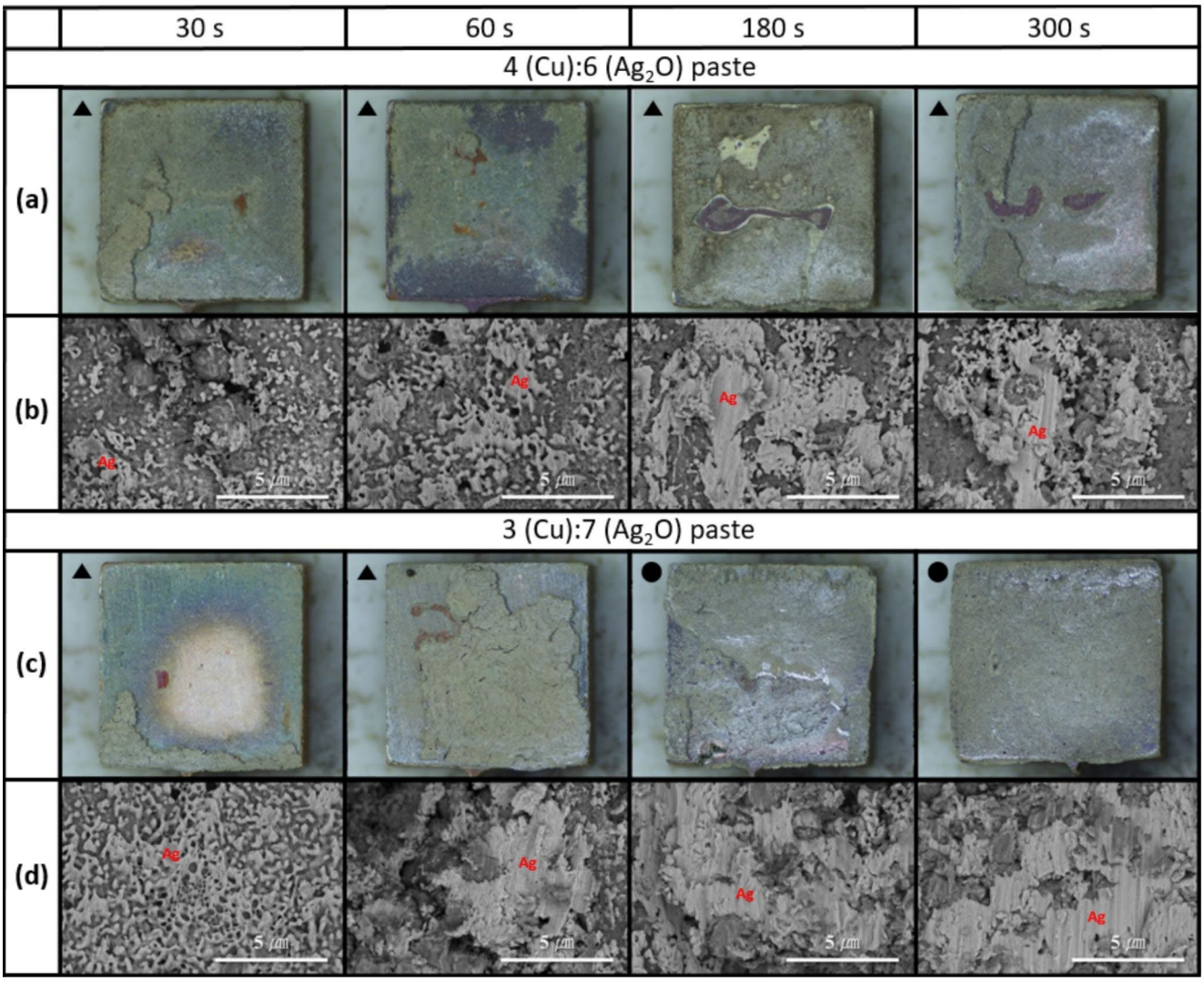

Fig. 9 **(a), (c)** Optical and **(b), (d)** BSE images of fracture surfaces formed on bond-lines by shearing. Sinter-bonding was performed under different particle mixing ratios and bonding times under 5 MPa compression at 300 °C in air: **(a), (b)** 6:4 and **(c), (d)** 3:7 ratios

Acknowledgements This study was supported by the Research Program (2022 – 0475) funded by the SeoulTech (Seoul National University of Science and Technology).

Declarations

Competing Interests The authors declare that they have no competing financial interests or personal relationships that could have influenced the work reported in this paper.

References

1. Chin, H.S., Cheong, K.Y., Ismail, A.B.: A review on die attach materials for SiC-based high-temperature power devices. Metall. Mater. Trans. B. **41B**, 824–832 (2010)
2. Zhang, H., Chen, C., Jiu, J., Nagao, S., Suganuma, K.: High-temperature reliability of low-temperature and pressureless micron Ag sintered joints for die attachment in high-power device. J. Mater. Sci. : Mater. Electron. **29**, 8854–8862 (2018)
3. Hong, W.S., Kim, M.S., Oh, C., Joo, Y., Kim, Y., Hong, K.-K.: Pressureless silver sintering of silicon-carbide power modules for electric vehicles. JOM. **72**, 889–897 (2020)
4. Hong, W.S., Kim, M.S., Oh, C.: Low-pressure silver sintering of automobile power modules with a silicon-carbide device and an active-metal-brazed substrate. J. Electron. Mater. **49**, 188–195 (2020)
5. Chen, T.F., Siow, K.S.: Comparing the mechanical and thermal-electrical properties of sintered copper (Cu) and sintered silver (ag) joints. J. Alloys Compd. **866**, 158783 (2021)
6. Ishihara, S., Takemasa, T., Suganuma, K., Kano, J.: Analysis of the formation mechanism of coarse-dense structure of silver paste in die bonding. Adv. Power Technol. **32**, 2020–2028 (2021)
7. Wang, F., Chen, H., Li, D., Zhang, Z., Wang, X.: Interfacial behaviors in Cu/molten Sn–58Bi/Cu solder joints under coupling with thermal and current stressing. Electron. Mater. Lett. **15**, 36–48 (2019)
8. Siswanto, W.A., Arun, M., Krasnopevtseva, I.V., Surendar, A., Maseleno, A.: A competition between stress triaxiality and joule heating on microstructure evolution and degradation of SnAgCu solder joints. J. Manufac Process. **54**, 221–227 (2020)

9. Zhang, B., Jabarullah, N.H., Alkaim, A.F., Danshina, S., Krasnopevtseva, I.V., Zheng, Y., Geetha, N.: Thermomechanical fatigue lifetime evaluation of solder joints in power semiconductors using a novel energy based modeling. Solder Surf. Mount Technol. **33**, 187–194 (2021)
10. Bakhshan, Y., Samari, F., Ghaemi, M., Ghafarigousheh, S., Kakoee, A.: Experimental study on the thermal conductivity of silver nanoparticles synthesized using Sargassum Angostifolium. Iran. J Sci Technol Trans Mech Eng. **43**, 5251–5257 (2019)
11. Lin, S., Nagao, S., Yokoi, E., Oh, C., Zhang, H., Liu, Y., Lin, S., Suganuma, K.: Nano-volcanic eruption of silver. Sci. Rep. **6**, 34769 (2016)
12. Wang, Q., Zhang, S., Lin, T., Zhang, P., He, P., Paik, K.-W.: Highly mechanical and high-temperature properties of Cu-Cu joints using citrate-coated nanosized ag paste in air. Prog Nat. Sci. : Mater. Int. **31**, 129–140 (2021)
13. Ide, E., Angata, S., Hirose, A., Kobayashi, K.F.: Metal–metal bonding process using Ag metallo-organic nanoparticles. Acta Mater. **53**, 2385–2393 (2005)
14. Zhang, S., Wang, Q., Lin, T., Zhang, P., He, P., Paik, K.-W.: Cu-Cu joining using citrate coated ultra-small nano-silver pastes. J. Manuf. Process. **62**, 546–554 (2021)
15. Fang, J.-P., Cai, J., Wang, Q., Zheng, K., Zhou, Y.-K., Geng, Z.-T.: Low temperature Au-Au bonding using ag nanoparticles as intermediate for die attachment in power device packaging. Appl. Surf. Sci. **593**, 153436 (2022)
16. Gao, R., Shen, Y.-A., Li, J., He, S., Nishikawa, H.: Mechanical and microstructural enhancements of Ag microparticle-sintered joint by ultrasonic vibration. J. Mater. Sci. : Mater. Electron. **31**, 21711 (2020)
17. Lee, Y.-J., Lee, J.-H.: Low–temperature and high–speed pressure–assisted sinter bonding using Ag derived by the redox reaction of ethylene glycol–based Ag_2O paste. Electron. Mater. Lett. **18**, 94–103 (2022)
18. Morita, T., Yasuda, Y., Ide, E., Akada, Y., Hirose, A.: Bonding technique using micro-scaled silver-oxide particles for in-situ formation of silver nanoparticles. Mater. Trans. **49**, 2875–2880 (2008)
19. Ogura, T., Yagishita, T., Takata, S., Fujimoto, T., Hirose, A.: Bondability of copper joints formed using a mixed paste of Ag_2O and CuO for low-temperature sinter bonding. Mater. Trans. **54**, 860–865 (2013)
20. Ogura, T., Takata, S., Takahashi, M., Hirose, A.: Effects of reducing solvent on copper, nickel, and aluminum joining using silver nanoparticles derived from a silver oxide paste. Mater. Trans. **56**, 1030–1036 (2015)
21. Asama, K., Matsuda, T., Ogura, T., Sano, T., Takahashi, M., Hirose, A.: Low-temperature metal-to-alumina direct bonding process utilizing redox reaction between silver oxide and organic agent. Mater. Sci. Eng. A. **702**, 398–405 (2017)
22. Mototama, K., Matsuda, T., Sano, T., Hirose, A.: AlN-to-metal direct bonding process utilizing sintering of Ag nanoparticles derived from the reduction of Ag_2O. J. Electron. Mater. **47**, 5780–5787 (2018)
23. Matsuda, T., Inami, K., Motoyama, K., Sano, T., Hirose, A.: Silver oxide decomposition mediated direct bonding of silicon-based material. Sci. Rep. **8**, 10472 (2018)
24. Choi, E.B., Lee, J.-H.: Sub-1 min sinter-bonding technique in air using modified Cu dendritic particles for formation of a high-temperature sustainable bondline. Met. Mater. Int. **27**, 5278–5284 (2021)
25. Choi, E.B., Lee, J.-H.: Tens-of-seconds solid-state sinter-bonding technique in air using in situ reduction of surface oxide layers on easily bendable dendritic cu particles. Appl. Surf. Sci. **580**, 152347 (2022)
26. Yong, N.L., Ahmad, A., Mohammad, A.W.: Synthesis and characterization of silver oxide nanoparticles by a novel method. Int. J. Sci. Eng. Res. **4**, 155–158 (2013)
27. Waterhouse, G.I.N., Bowmaker, G.A., Metson, J.B.: The thermal decomposition of silver (I, III) oxide: A combined XRD, FT-IR and Raman spectroscopic study. Phys. Chem. Chem. Phys. **3**, 3838–3845 (2001)
28. Simo, A., Polte, J., Pfänder, N., Vainio, U., Emmerling, F., Rademann, K.: Formation mechanism of silver nanoparticles stabilized in glassy matrices. J. Am. Chem. Soc. **134**, 18824–18833 (2012)
29. Kim, I., Chun, S.: Effects of solvent type on low-temperature sintering of silver oxide paste to form electrically conductive silver film. J. Electron. Mater. **40**, 1977–1983 (2011)
30. Suganuma, K., Kim, S.-J., Kim, K.-S.: High-temperature lead-free solders: Properties and possibilities. JOM. **61**, 64–71 (2009)
31. Siow, K.S., Manikam, V.R., Chua, S.T.: Process control of sintered ag joint in production for die attach applications. In: Siow, K.S. (ed.) Die-attach Materials for high Temperature Applications in Microelectronics Packaging, pp. 67–105. Springer Cham (2019)
32. Kim, J.H., Lee, J.-H.: Microstructural investigation of the oxidation behavior of Cu in Ag-coated Cu films using a focused ion beam transmission electron microscopy technique. Jpn J. Appl. Phys. **55**, 06JG01 (2016)